

Ferromagnetic Nanostructures by Atomic Layer Deposition: From Thin Films towards Core-shell Nanotubes

M. Daub¹, J. Bachmann¹, J. Jing¹, M. Knez¹, U. Gösele¹, S. Barth³,
S. Mathur³, J. Escrig^{1,4}, D. Altbir⁴ and K. Nielsch^{1,2}

¹Max Planck Institute for Microstructure Physics, Halle (Germany)

²Present Address: Institute of Applied Physics, University of Hamburg (Germany)

³Leibniz-Institut für Neue Materialien, CVD Division, Saarbruecken (Germany)

⁴Departamento de Física, Universidad de Santiago (Chile)

Abstract

Nickel, cobalt and iron oxide nanotubes were obtained by atomic layer deposition (ALD) into the pores of alumina membranes. Initially, a metal oxide film was grown by the reaction of a precursor vapor of NiCp₂ (nickelocene), CoCp₂ (cobaltocene) or FeCp₂ (ferrocene) with ozone, respectively. Subsequently, the metal oxide film was reduced in hydrogen atmosphere and converted to a metallic ferromagnetic phase with low-degree of surface roughness. In a similar manner, Fe₃O₄ films have also been obtained by the atomic layer deposition of Fe₂O₃ films based on the reaction of water and iron(III) *tert*-butoxide (Fe₂(O^{*t*}Bu)₆), followed by a hydrogen reduction to Fe₃O₄ after the ALD process. By conformal coating of self-ordered Al₂O₃ membranes, arrays of magnetic nanotubes with diameters down to 30 nm and wall thicknesses of less than 3 nm have been achieved. The magnetic properties of the nanotube arrays as a function of wall thickness and tube diameter have been studied by SQUID magnetometry. Atomic layer deposition (ALD) was proven to be a very suitable method for the conformal deposition of magnetic thin films in pore structures of high aspect ratio, while offering high uniformity and precise tuning of the layer thickness and the magnetic properties.

Introduction

A broad range of potential applications of patterned magnetic nanostructures, such as arrays of wires, tubes, stripes or rings, have been developed in recent years¹⁻⁴. Magnetic data storage, microelectronics, or biomedical processes such as cell separation or biosensing attract special interest. Among the different types of nanostructures, tubes offer an additional degree of freedom as compared to nanowires, in that not only the length and diameter can be varied, but also the thickness of the tube walls. Changes in thickness are expected to strongly affect the mechanism of magnetization reversal and thereby the overall magnetic response^{5,6}. The synthesis of magnetic tubular nanostructures has until now mainly been performed by using porous templates, such as anodic alumina or ion track-etched membranes. Ni and Co nanotubes have been fabricated by silanization and electrochemical deposition in polycarbonate or alumina membranes.^{7,8,9} Co, Fe, CoNiFe/Cu and Ni nanotubes were produced by pulsed electrodeposition^{10,11} or by dc electrodeposition¹², Au/Ni multilayer nanotubes were fabricated by coating alumina walls with Ag nanoparticles and subsequent electrodeposition.¹³ Precursor injection and subsequent hydrogen reduction were used for the fabrication of FePt and FePt/Fe nanotubes.^{14,15} Co nanotubes were fabricated by

wetting the pores of alumina membranes with a polystyrene/poly-l-lactide solution containing a metallo-organic precursor and annealing.¹⁶ Most of the previous papers report the formation of nanotubes with relatively large diameters (200-300 nm). In addition, these methods do not allow for precise control of the layer thickness and fine tuning of the magnetic properties.

In this paper we report the fabrication of highly conformal nickel and iron oxide nanotubes in porous alumina templates by atomic layer deposition (ALD) on the pore walls of alumina membranes. ALD is a very suitable method for the conformal deposition of magnetic thin films onto structures with high aspect ratio, while offering the precise tuning of the layer thickness and high uniformity^{17,18}. ALD is used for the deposition of thin layers from two different vapour-phase reactants by subsequently exposing the substrate to the precursor vapours. This exposing cycle leads to usually one monolayer or less of the material of choice and should be repeated several times until the desired film thickness is reached.

Experimental

Alumina membranes with 100 nm and 500 nm interpore distances, pore diameters of 35 nm and 160 nm, and pore lengths of 2-50 μm were fabricated in a two-step anodization process of aluminum¹⁹⁻²¹. For obtaining pore diameters of 55-85 nm, we treated the samples in 5% H_3PO_4 at 30 °C for 30-60 minutes. The alumina membranes were used as templates for the ALD deposition of Ni, Co and Fe_2O_3 .

ALD was carried out in a Savannah 100 system from Cambridge Nanotech operating with Ar as carrier gas. The precursors were kept in sealed Swagelok stainless steel bottles that were thoroughly degassed before use. We used nickelocene (NiCp_2), cobaltocene (CoCp_2) or ferrocene (FeCp_2), all from Strem Chemicals, as precursors for atomic layer deposition. The deposition process consists of two steps: first, the nickelocene, cobaltocene or ferrocene vapour forms a sub-monolayer on the sample surface; then, ozone is introduced into the ALD chamber to react with the adsorbed layer. This cycle is repeated several times, in order to achieve the desired layer thickness. After the deposition process, the sample with the metal oxide coating is transferred into an oven (Ulvak-Riko Mila 3000) and reduced at 400 °C in Ar + 5% H_2 atmosphere for 5 hours. For Ni, the deposition temperature ranged between 270 °C and 330 °C and for Co, between 240 °C and 330 °C at 2×10^{-1} Torr. The deposition of iron oxide was performed at 200°C. The precursor temperature was in all cases 90 °C. Pulsing time of 1 s, exposure time of 20-30 s and purging time (Ar gas, flow rate of 10 sccm) of 20-30 s were used for all ALD cycles.

For atomic layer deposition of Fe_2O_3 , water and the homoleptic dinuclear iron(III) *tert*-butoxide complex, $\text{Fe}_2(\text{O}^t\text{Bu})_6$ were also used²²⁻²⁴. $\text{Fe}_2(\text{O}^t\text{Bu})_6$ was synthesized according to published procedures and handled in inert atmosphere. When the $\text{Fe}_2(\text{O}^t\text{Bu})_6$ precursor was heated to 100°C, a temperature window was found between 130 and 170°C in which a linear growth of the deposit was observed. At lower temperatures, deposition does not occur as judged from the absence of color change. The onset of $\text{Fe}_2(\text{O}^t\text{Bu})_6$ thermal decomposition sets the upper limit of ALD. The exact chemical identity of the pore walls

was controlled by depositing a 5-nm layer of Al_2O_3 by ALD (by hydrolysis of $\text{Al}(\text{CH}_3)_3$) before the Fe_2O_3 deposition. Reduction of the tubes to Fe_3O_4 ^{25,26} was performed subsequently by heating the $\text{Al}_2\text{O}_3 / \text{Fe}_2\text{O}_3$ composites to 400°C in the oven in 1 atm of $\text{Ar} + 5\% \text{H}_2$ for 12 hr. After cooling under H_2 / Ar , the samples were quickly transferred to a glovebox (MBraun) operating with N_2 . They were then covered by a thin protective film of molten polystyrene (PS) at 180°C . After cooling down to room temperature, they were handled in air. The nanotubes obtained by hydrolyzing the *t*-butoxide were preferred for magnetic measurements because the lower deposition temperature favors smoother films. Figure 1 shows the schematic representation of experimental procedures for Fe_2O_3 .

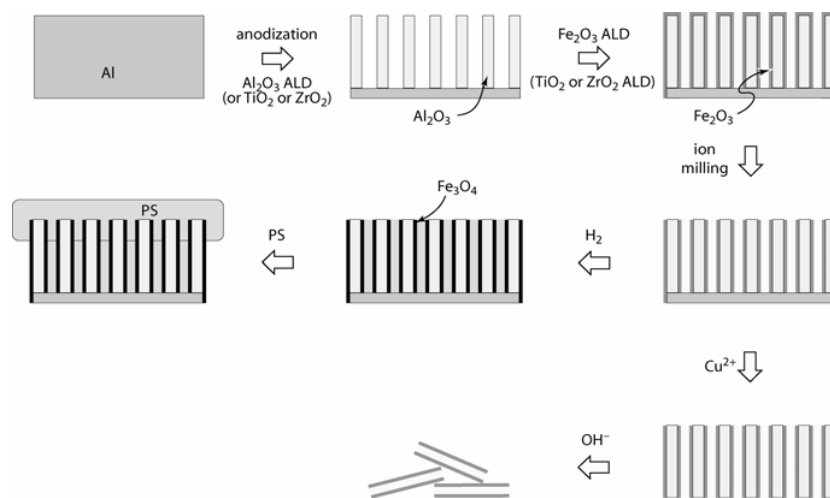


Figure 1: Scheme of the procedure steps for atomic layer deposition of Fe_2O_3 .

For the SEM, TEM and magnetic measurements, the alumina surface was treated by an ion milling process to remove the deposited film from the top sample surface. For a higher stability of the nanotubes and to prevent damaging of the nanotubes by the etching solution, we deposited TiO_2 ²⁷ or ZrO_2 (by ALD using the hydrolysis reaction of $\text{Ti}(\text{O}^i\text{Pr})_4$ or $\text{Zr}(\text{O}^i\text{Bu})_4$, respectively), prior to the deposition of magnetic films. An additional layer of the same thickness and same material was subsequently deposited onto the nickel, cobalt or iron oxide tubes. After ion milling, the Al backside of the TiO_2 - or ZrO_2 -coated magnetic nanotubes was dissolved in acidic CuCl_2 solution and the alumina membrane in concentrated aqueous NaOH , followed by rinsing with H_2O until $\text{pH} \leq 10$. The nanotubes were placed on a TEM sample holder consisting of a Cu grid and a holey C film (Plano, Wetzlar) by evaporating a droplet of the suspension on the grid.

Ion milling was performed on squares of $\approx 5\text{-}10 \text{ mm}^2$ area cut from the alumina membrane, using a Dual Ion Mill machine (Gatan, model 600). Ar^+ ions (0.5 mA) were accelerated under 4 kV and directed onto the sample under a 20° angle. Ion milling was typically conducted for 5-10 minutes per sample. SEM micrographs were taken with a Jeol JSM 6300F at acceleration voltages ranging between 2.5 and 15 kV. Low acceleration voltages were usually required due to the poor electrical conductivity of the samples. TEM data were collected on a Jeol JEM 1010 operating at 100 kV. Magnetic properties of the nanotube arrays as a function of wall thickness and tube diameter were investigated using a QuantumDesign MPMS-XL SQUID magnetometer.

Step	SQUID	SEM/TEM
1	Anodization of alumina membranes	Anodization of alumina membranes
2	-	ALD of TiO ₂ / ZrO ₂
3	ALD of NiO, CoO, Fe ₂ O ₃	ALD of NiO, CoO, Fe ₂ O ₃
4	-	ALD of TiO ₂ / ZrO ₂
5	Ion milling	Ion milling
6	Reduction at 400 °C in Ar + 5% H ₂	Reduction at 400 °C in Ar + 5% H ₂
7	Polystyrene coverage	Etching of Al ₂ O ₃ and Al

Table 1. Process sequence for the preparation of samples for SEM/TEM and SQUID measurements.

Results and Discussion

Figure 2a shows scanning electron micrographs of TiO₂ /Ni/TiO₂ tubes obtained with 500 ALD cycles at 330 °C (layer thickness of about 11–12 nm). The measured grain size was less than 5 nm, this morphology of the multilayer TiO₂/Ni/TiO₂ tubes being also confirmed by TEM measurements. The Ni tubes presented in Fig. 2b were also obtained by 500 ALD cycles and have the same layer thickness and pore length (10 μm) as the nanotubes presented in Figure 2a. The first TiO₂ layer has a thickness of about 10 nm, and the second TiO₂ layer of about 5 nm. We studied by means of SEM and TEM tubes with two different diameters: 35 or 160 nm. We chose for Figure 2a and b samples with pore diameters of 160 nm for better clarity and quality of the microscopy images.

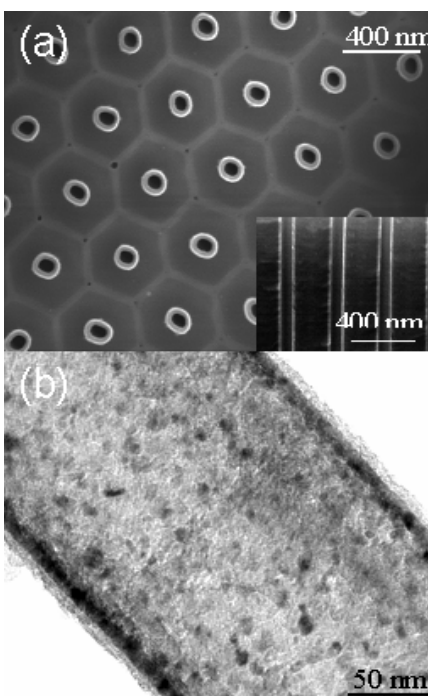


Figure 2: a) SEM top-view image for an alumina membrane containing TiO₂/Ni/TiO₂ nanotubes (inset: cross-section view of the membrane); b) typical TEM results for TiO₂/Ni/TiO₂ nanotubes.

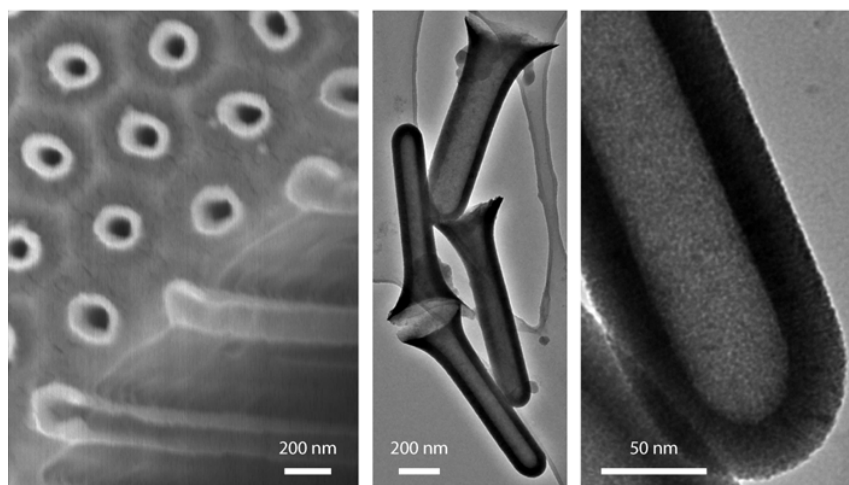


Figure 3: Electron micrographs of iron oxide nanotubes. Left: scanning electron micrograph of an array of parallel $\text{ZrO}_2 / \text{Fe}_3\text{O}_4 / \text{ZrO}_2$ tubes embedded in the alumina matrix (after Ar^+ ion milling and a short KOH etch); the view is taken at a crack in the membrane, showing both the hexagonally arranged tube ends emerging on the top side of the membrane and tubes broken in halves in their length, traversing the membrane. Center and right: transmission electron micrographs of isolated short Fe_3O_4 tubes (obtained by ALD of $\text{Fe}_2(\text{O}^t\text{Bu})_6$) after complete dissolution of the alumina matrix in KOH solution.

Recently, ALD processes have been developed for magnetic thin films. Due to the low reactivity of molecular hydrogen, most processes for transition metals, like Ni and Co, based on the reaction of H_2 and a metal-organic precursor, are rather slow (0.04–0.12 Å/cycle). Deposition rates of 0.22–0.3 Å/cycle for both nickel and iron oxide lead us to obtain very uniform and conformal nanostructures.²⁸⁻³¹ On the other hand, we observed that the direct reaction of a metal-organic precursor and hydrogen during the ALD cycle always yields very granular films with ill-defined magnetic properties (very small coercivities, < 30 Oe) and very low deposition rates (< 0.1 Å/cycle).

The magnetic properties of Ni nanotubes with different diameters and magnetic layer thicknesses were measured with a superconducting quantum interference device (SQUID) magnetometer. Typical coercivities for Ni nanotubes of 35 nm diameter are 190 Oe for the parallel configuration and 90 Oe for the perpendicular configuration (1 Oe = $10^3/4\pi$ Am⁻¹). The coercivities obtained for Co nanotubes of similar dimensions are 550 Oe for the parallel direction and 390 Oe for the perpendicular direction (Figure 4). For pore diameters of around 160 nm, the Ni and Co nanotubes showed a nearly isotropic behavior, with coercivities in both measurement configurations of around 100 Oe for Ni and 580 Oe for Co. The coercivities measured in our samples were in the same range of values than other results reported in literature^{1,6}. As a comparison, the coercivity values for bulk are much smaller (< 10 Oe for Ni; around 10 Oe for Co). Due to the shape anisotropy, the nanotubes with smaller diameters (around 35 nm) show enhanced coercivities and anisotropic magnetic behavior. For these samples, the remanent magnetization for an external field applied parallel to the tube axis is larger than that for

the perpendicular direction, indicating that the easy axis of magnetization is oriented along the nanotube axis. The preferential arrangement of the magnetic moments is the parallel (ferromagnetic) configuration for smaller diameters (<80 nm) and a vortex state for the larger diameter nanotubes (>100 nm).⁵

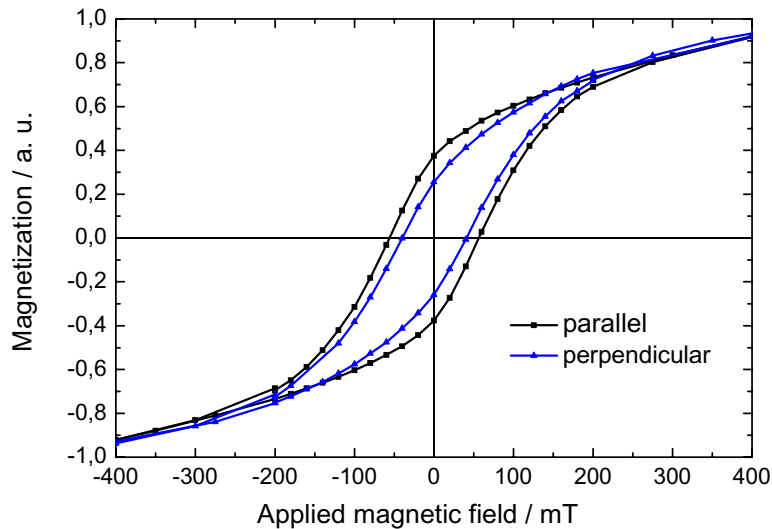


Figure 4: Typical hysteresis cycles for Co nanotubes of 35 nm diameter and less than 5 μm pore length, Co layer thickness around 10 nm; the magnetic field is applied parallel or perpendicular to the nanotube axis.

The influence of the pore diameter or of the layer thickness on the magnetic properties was also investigated. Figure 5 shows the hysteresis cycles for five different samples with diameters of 35, 55, and 85 nm, which were deposited with the same number of ALD cycles, corresponding to 11–12 nm Ni thickness. For the samples with a nominal pore diameter of 35 nm, the Ni layer thickness was varied as follows: 3–4 nm, 6–7 nm and 11–12 nm. The interpore distance was in all cases 100 nm and the pore length of around 30 μm . We observed that when the pore diameter decreases, the coercivity and the remanence increase - and the saturation magnetization decreases. By increasing the number of ALD cycles (150, 300, and 500 cycles, corresponding to 3–4, 6–7, and 11–12 nm thickness), we obtain an increase in the saturation magnetization and coercivity.

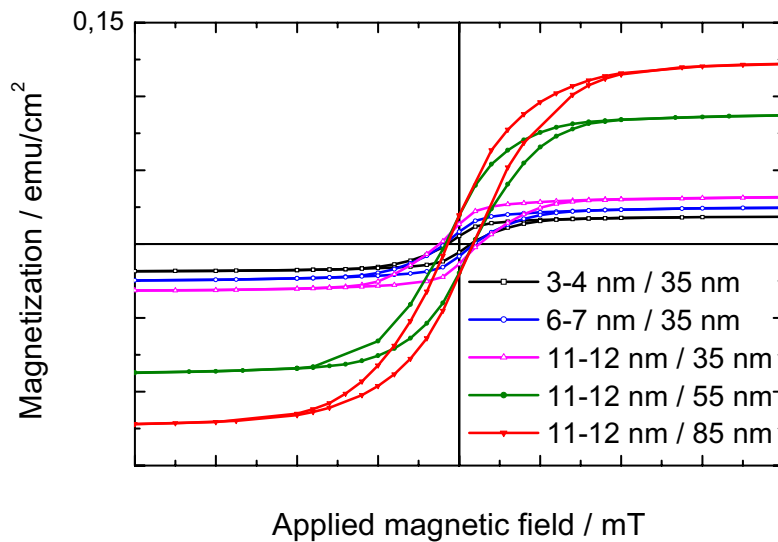


Figure 5: Hysteresis loops for nanotubes with different Ni layer thickness: 3–4 nm, 6–7 nm, and 11–12 nm and different pore diameters: 35 nm, 55 nm and 85 nm. The magnetic field was applied parallel to the nanotube axis.

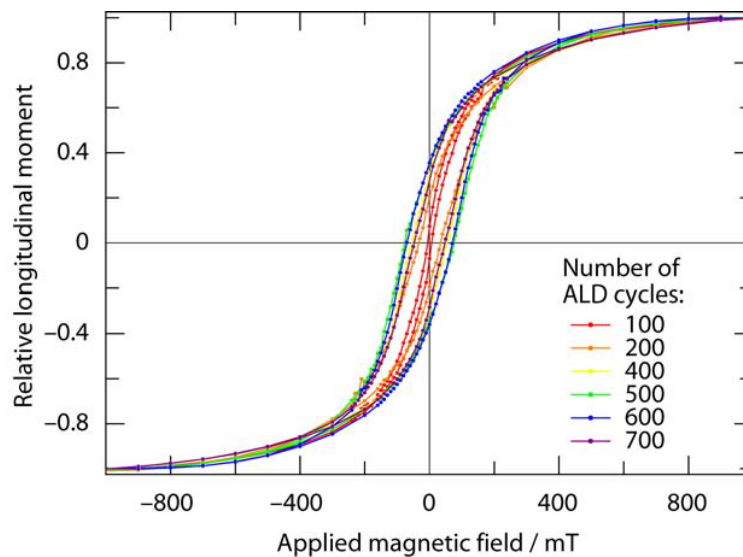


Figure 6. Magnetic hystereses of Fe_3O_4 nanotube arrays, obtained with $\text{Fe}_2(\text{O}^i\text{Bu})_6$, of various wall thicknesses d_w in a field applied parallel to their long axis. Geometric parameters of the tubes: outer diameter 50 nm, center-to-center distance 105 nm, length 3 μm , wall thickness d_w between 2.6 nm (red) and 18.2 nm (purple). The growth rate of the wall thickness d_w is approximately 2.6 nm for 100 ALD cycles. For each hysteresis, a paramagnetic background has been subtracted from the curve, and then the data have been normalized to the signal at 1 T. The largest remanence and coercive field are obtained for $d_w = 13$ nm (500 ALD cycles, green curve).

The outstanding control over the wall thickness of our iron oxide nanotubes afforded by ALD allows the magnetic properties to be systematically studied as a function of geometry, as shown in Figure 6. For a constant external diameter of the nanotubes (50 nm), coercivity H_c and remanence strongly depend on the wall thickness d_w . In the limit of very thin walls, the tubes behave as soft ferromagnets with vanishing coercivity ($H_c^{100} = 50$ Oe)¹ and remanence. Both of those parameters then increase with d_w up to $d_w = 13$ nm approximately ($H_c^{500} = 770$ Oe). Further increases in d_w are accompanied by receding remanence and coercivity ($H_c^{700} = 470$ Oe).

The observation that geometric parameters can be used to tune and even optimize the magnetic response of nanostructures is of importance for the design of future high-density magnetic data storage systems. More fundamentally, it reflects the complexity of magnetic phenomena happening on the length scales between 10 nm and 1 μ m. At small Zeeman energies, the competition between different magnetization reversal modes of similar energy may be significantly affected by factors such as the magnetic coupling between neighboring tubes, structural irregularities and geometric inhomogeneities of the tubes, and surface effects.

The magnetic characterization of Ni nanotubes obtained by ALD presented similar values for coercivity, saturation magnetization and remanence magnetization as Ni nanotubes obtained by other methods and published until now in the literature^{1,6}. However, the precise study in nanometer range of the influence of Ni layer thickness on the magnetic properties is, to our knowledge, for the first time made possible by using ALD. Atomic layer deposition allows a very precise control of the layer thickness, a fine tuning of the magnetic properties and a very conformal and uniform coverage of the substrate.

The two ALD reactions for the deposition of Fe_2O_3 ($Fe_2(O^tBu)_6 + H_2O$ and $Cp_2Fe + O_3$) are diametrically opposed in many respects, and thereby favorably complement each other. The former is a chemically well-defined hydrolysis, while the latter bases on a combustion, a type of reaction that occurs via a multiplicity of intermediates and pathways and is therefore less controlled. Accordingly, the hydrolysis can be performed with similar results over a relatively wide range of temperatures (at least 50°C), whereas we have observed that the combustion is only reproducible if the temperature of the sample remains constant between subsequent runs. On the other hand, the precursor ferrocene present several practical advantages over iron(III) *tert*-butoxide, in particular thermal and aerobic stability, commercial availability, better volatility. Finally, the different deposition temperatures required by the two reactions have two consequences. The relatively low substrate temperature associated with the hydrolysis favors a structurally amorphous state of the deposited layer, which yields very smooth thin films. The higher temperature of the oxidation process, however, speeds up diffusion of the gaseous precursors and thus allows the ALD conditions to be met in substrates of higher porosity.

¹ Let H_c^x designate the coercive field of tubes obtained by x ALD cycles.

Conclusions

Nickel, iron oxide and cobalt nanotubes were produced in alumina membranes with different pore diameters by Atomic Layer Deposition. Nickelocene, cobaltocene, ferrocene and a homoleptic dinuclear iron(III) tert-butoxide complex were used as first precursors, and ozone or water as second precursors. The magnetic nanotubes were investigated by SEM, TEM and SQUID. We obtained very uniform and conformal nanostructures with deposition rates of 0.22–0.3 Å/ cycle. The method of atomic layer deposition offers a very precise control of layer growth and, thus, a high degree of flexibility in the fabrication of 3D nanostructures with desired ferromagnetic properties.

Acknowledgment

We appreciate financial support by the German Ministry of Science and Education, BMBF, via Research Contract FKZ 03N8701. J. Bachmann acknowledges the A. von Humboldt Foundation for a postdoctoral fellowship (3-SCZ/1122413 STP).

References

1. Whitney, T. M.; Jiang, J. S.; Searson, P. C.; Chien, C. L. *Science* 1993, 261, 1316-1319.
2. Prinz, G. A. *Science* 1998, 282, 1660-1663.
3. Thurn-Albrecht, T.; Schotter, J.; Kastle, C. A.; Emley, N.; Shibauchi, T.; Krusin-Elbaum, L.; Guarini, K.; Black, C. T.; Tuominen, M. T.; Russell, T. P. *Science* 2000, 290, 2126-2129.
4. Nielsch, K.; Wehrspohn, R. B.; Barthel, J.; Kirschner, J.; Gösele, U.; Fischer, S. F.; Kronmüller, H. *Appl. Phys. Lett.* 2001, 79, 1360-1362.
5. Escrig, J.; Landeros, P.; Altbir, D.; Vogel, E. E.; Vargas, P. *J. Magn. Magn. Mat.* 2007, 308, 233-237.
6. Sui, Y. C.; Skomski, R.; Sorge, K. D.; Sellmyer, D. *J. Appl. Phys. Lett.* 2004, 84, 1525-2527.
7. Bao, J.; Tie, C.; Xu, Z.; Zhou, Q.; Shen, D.; Ma, Q. *Adv. Mater* (Weinheim, Ger.), 2001, 13, 1631.
8. Xue, S.; Cao, C.; Zhu, H. *J. Mater. Sci* 2006, 41, 5598.
9. Bao, J.; Xu, Z.; Hong, J.; Ma, X.; Lu, Z. *Scr. Mater.* 2004, 50, 19.
10. Tourillon, G; Pontonnier, L; Levy, J.P; Langlais, P. *Electrochem. Solid-State Lett.* 2000, 3, 20.
11. Davis, D.M.; Moldovan, M.; Young, D.P.; Henk, M; Xie, X.; Podlaha, E.J. *Electrochem. Solid-State Lett.* 2006, 9, C153.
12. Tao, F.; Guan, M.; Jiang, Y.; Zhu, J.; Xu, Z.; Xue, Z. *Adv. Mater.* 2006, 18, 2161.
13. Lee, W.; Scholz, R.; Nielsch, K.; Goesele, U. *Angew. Chem. Int. Ed.* 2005, 44, 6050.
14. Sui, Y.C.; Skomski, R.; Sorge, K. D.; Sellmyer, D. J. *J. Appl. Phys.* 2004, 95, 7151.
15. Su, H.L.; Tang, S.L.; Tang, N.R.; Wang, L.; Lu, M.; Du, Y.W. *Nanotechnology* 2005, 16, 2124.

16. Nielsch, K.; Castano, F.J.; Ross, C.A.; Krishnan, R. *J. Appl. Phys.* 2005, 98, 034318
17. Puurunen, R. L. *Appl. Phys. Rev.* 2005, 97, 121301.
18. Knez, M.; Nielsch, K.; Niinistö, L. *Adv. Mat.* 2007, accepted.
19. Masuda, H.; Yada, K.; Osaka, A. *Jpn. J. Appl. Phys. Part 2* 1998, 37, L1340.
20. Nielsch, K.; Choi, J.; Schwirn, K.; Wehrspohn, R.B.; Goesele, U. *Nano Lett.* 2002, 2, 677.
21. Nielsch, K.; Castano, F.J.; Matthias, S.; Lee, W.; Ross, C.A.; *Adv. Eng. Mater.* 2005, 7, 217.
22. Mathur, S.; Veith, M.; Sivakov, V.; Shen, H.; Huch, V.; Hartmann, U.; Gao, H. B. *Chem. Vap. Depos.* 2002, 8, 277-283.
23. Spandl, J.; Kusserow, M.; Bruedgam, I. *Z. Anorg. Allg. Chem.* 2003, 629, 968-974.
24. Mathur, S.; Sivakov, V.; Shen, H.; Barth, S.; Cavelius, C.; Nilsson, A.; Kuhn, P. *Thin Solid Films* 2006, 502, 88-93.
25. Regazzoni, A. E.; Urrutia, G. A.; Blesa, M. A. Maroto, A. J. G. *J. Inorg. Nucl. Chem.* 1981, 43, 1489-1493.
26. Jiao, F.; Jumas, J. C.; Womes, M.; Chadwick, A. V.; Harrison, A.; Bruce, P. G. *J. Am. Chem. Soc.* 2006, 128, 12905-12909.
27. Knez, M.; Kadri, A.; Wege, C.; Gosele, U.; Jeske, H.; Nielsch, K. *Nano Lett.* 2006, 6, 1172.
28. Lim, B.S.; Rahtu, A.; Gordon, R.G.; *Nat. Mater.* 2003, 2, 749.
29. Chae, J.; Park, H.S.; Kang, S.W. *Electrochem. Solid-State Lett.* 2002, 5, C64.
30. Utriainen, M.; Kröger-Laukkanen, M.; Johansson, L.S.; Niinisto, L. *Appl. Surf. Sci.* 2000, 157, 151.
31. Utriainen, M.; Kröger-Laukkanen, M.; Niinisto, L. *Mat. Sci. Eng. B* 1998, 54, 98.